Athenea

Revista en Ciencias de la Ingeniería

ISSN: 2737-6439
DOI: 10.47460/athenea
Volume 5, Issue 15
March 2024

Published by:

AutanaBooks
Engineering & Services

ATHENEA JOURNAL

JOURNAL IN ENGINEERING SCIENCES

Electronic Journal Edited By AutanaBooks.

Quarterly Periodicity

Our cover:

Athenea, Engineering Sciences Magazine is pleased to bring a new issue where it continues to support Latin American research.

Volume 5 // Issue 15 // JAN-MAR 2024
DOI:10.47460/athenea
ISSN: 2737-6439

Viewing the Journal:
https://athenea.autanabooks.com/index.php/revista

TECHNICAL TEAM

Webmaster and Metadata
Ing. Ángel Lezama (Quito, Ecuador).
a2lezama@gmail.com

Graphic design and layout:
Adrián Hauser
(AutanaBooks, Ecuador).
adrian.hauser@gmail.com

Translator: Fausto Bartolotta
Via Francesco Crispi, 309/A
98028 Santa Teresa Di Riva, Provincia Messina
Italia
email: fbartolotta@gmail.com

"by the grace of God"

Publisher: Dr. Franyelit Suárez,
http://orcid.org/0000-0002-8763-5513
editorial@autanabooks.com
AutanaBooks, Quito, Ecuador

DIRECTORY OF THE ATHENEA
JOURNAL IN ENGINEERING SCIENCES

ACADEMIC COMMITTEE

Athenea Journal
Volume 5 // Issue 15 // December 2024
DOI:10.47460/athenea/v5i15
ISSN: 2737-6439

Content

Editorial

In an industrial world with permanent technological changes and increasingly demanding societies, the tireless search for efficient and sustainable energy solutions has led to exploring the limits of science and technology. In this edition of our magazine, we delve into three fundamental areas that are shaping the energy landscape of the future: the simple pendulum, photovoltaic plants, and thermoelectric materials. On the one hand, the simple pendulum, from its early days as an object of study in classical physics to its application in contemporary science, has exemplified the elegance of simplicity in physical analysis. Its oscillatory motion, governed by precise laws, has served as a cornerstone for understanding fundamental concepts in mechanics and dynamics. However, its relevance transcends the theoretical; The simple pendulum finds practical applications in a variety of fields, from geophysics to sensor technology, demonstrating its versatility and usefulness in modern exploration and engineering.

On the other hand, photovoltaic plants represent a milestone in the search for renewable energy sources. These vast arrays of solar cells converge sunlight into clean, sustainable electrical currents, powering our societies with an inexhaustible energy source. As photovoltaic technology advances, solar plants are becoming pillars of global energy infrastructure, offering a viable alternative to fossil fuels and mitigating the effects of climate change. Finally, thermoelectric materials represent an interesting frontier in converting thermal energy into electricity. Using the Seebeck effect, these materials transform temperature differences into electrical currents, opening new possibilities in energy generation and cooling. From applications in space to wearable devices, thermoelectric materials promise to revolutionize the way we harness and use heat in our daily lives.

Athenea Journal, specializing in science and engineering, is pleased to publish volume 5, Issue 15, with a select group of research that provides a significant contribution to the study of engineering.

Dr. Franyelit Suárez


Athenea
Revista en Ciencias de la Ingeniería
ISSN: 2737-6439
DOI: 10.47460/athenea
Volume 5, Issue 15
March 2024
Published by:
AutanaBooks
Engineering & Services

ISSN-e: 2737-6419

Athenea Journal
Vol.5, Issue 15, (pp. 8-15)

https://doi.org/10.47460/athenea.v5i15.70

Statistical analysis in engineering practices

Juan Andrés Serrano Granja
https://orcid.org/0009-0007-6582-1896
juan.serrano.granja@udla.eu.ec
Universidad de las Américas
Carrera de Ingeniería de Software
Quito, Ecuador

Andrea Camila Manangón Palacios
https://orcid.org/0009-0001-1142-5800
andrea.manangon@udla.edu.ec
Universidad de las Américas
Carrera de Ingeniería de Software
Quito, Ecuador

Thommy Elián Calderón Mera
https://orcid.org/0009-0009-9209-4932
thommy.calderon@udla.edu.ec
Universidad de las Américas
Carrera de Ingeniería de Software
Quito, Ecuador

Daniel Adrian Sánchez Proaño
https://orcid.org/0009-0006-9849-2235
daniel.sanchez.proano@udla.edu.ec
Universidad de las Américas
Carrera de Ingeniería de Software
Quito, Ecuador.

Alexander Javier Sánchez Vinueza
https://orcid.org/0009-0002-4917-0548
alexander.sanchez.vinueza@udla.edu.ec
Universidad de las Américas
Carrera de Ingeniería de Software
Quito, Ecuador.

Roberto Andrés Zurita Molina
https://orcid.org/0009-0003-4428-7787
roberto.zurita.molina@udla.edu.ec
Universidad de las Américas
Carrera de Ingeniería de Software
Quito, Ecuador.

Received (20/09/2023), Accepted (23/01/2024)

Abstract. - In this project, an engineering experiment was conducted utilizing measurements to estimate gravity analytically and graphically. This experimental approach aims to demonstrate the usefulness of engineering principles in verifying Earth's gravity values. Statistical methods were employed to enhance comprehension of the underlying concepts and ensure precise error estimation. The principal findings suggest that this engineering practice is an effective tool for evaluating gravity, with descriptive statistical analysis playing a pivotal role in presenting dependable and precise data.

Keywords: gravity estimation, statistical methods, error analysis, experimental engineering.

Análisis estadístico en prácticas de ingeniería

Resumen: En este proyecto se realizó un experimento de ingeniería utilizando mediciones para estimar la gravedad analítica y gráficamente. Este enfoque experimental pretende demostrar la utilidad de los principios de ingeniería para verificar los valores de la gravedad terrestre. Se emplearon métodos estadísticos para mejorar la comprensión de los conceptos subyacentes y garantizar una estimación precisa de los errores. Los principales resultados sugieren que esta práctica de ingeniería es una herramienta eficaz para evaluar la gravedad, en la que el análisis estadístico descriptivo desempeña un papel fundamental a la hora de presentar datos fiables y precisos.

Palabras clave: estimación de gravedad, métodos estadísticos, análisis de errores, ingeniería experimental.

I. INTRODUCTION

As a fundamental discipline for solving problems and creating innovative solutions, engineering encompasses widespread fields and applications [1]. From building infrastructure to designing technological devices, engineers employ a combination of scientific knowledge and practical skills to address different challenges in our modern society. Within the realm of engineering practice, measurement, and data analysis constitute fundamental pillars in the evaluation and enhancement of systems and processes [2]. Within this framework, statistics emerges as a critical instrument enabling engineers to extract meaningful insights from datasets, discern patterns, and formulate well-informed decisions.

Statistics have a critical role, particularly in estimating physical parameters, like Earth's gravity [4]. Precise determination of this value underpins numerous engineering applications [3], ranging from structural construction to satellite navigation. Accurate measurements are essential to guarantee the safety and functionality of the systems and devices that rely on them. Consequently, engineers prioritize experimental practices designed to measure and verify gravity values. These experiments not only aim to acquire accurate data but also to validate and refine the measurement methods themselves. Additionally, this approach fosters a deeper understanding of the factors influencing this fundamental physical phenomenon [5].

In this context, statistical techniques become essential for analyzing the data obtained during experimental practices. A proper application of statistical methods allows engineers to calculate not only average gravity values but also evaluate the precision of measurements, identify potential sources of error, and improve results obtained reliability. Therefore, this study focuses on spotlighting the importance of statistics in engineering practices, specifically in the measurement and evaluation of the gravity of Earth. Through the performance of controlled experiments and the statistical analysis of the data collected, the aim is to demonstrate the effectiveness of statistical methods in obtaining accurate and reliable results, which are fundamental for the development and successful applications of engineering solutions in various areas.

II. DEVELOPMENT

Engineering internships are essential for several reasons. Firstly, it provides students and professionals with the opportunity to apply the theoretical knowledge acquired in a practical and realistic environment. This allows them to understand better the concepts and theories learned in the classroom by seeing how they are applied in real-world situations [6]. In addition, engineering internships encourage the development of practical skills and technical skills. Students can work with tools, equipment, and technologies used in the industry, which helps them gain hands-on experience that cannot be gained simply through theoretical teaching. Another important aspect is that internships in engineering provide the opportunity to work in multidisciplinary teams and collaborate with professionals from different areas. This helps students develop communication, teamwork, and problem-solving skills, all of which are essential for success in the engineering field.

Additionally, internships are a great way to network and develop professional networks. Students have the opportunity to interact with industry professionals, meet potential employers, and learn about the latest trends and advancements in the engineering field. In this sense, it can be said that engineering internships are fundamental for the comprehensive training of students since they provide them with practical experience, help them develop technical and professional skills, and allow them to establish contacts in the industry.

A. Critical Thinking and Practical Activity in Engineering

Critical thinking is a fundamental skill in engineering and is actively exercised during the execution of practical activities. In engineering it is not enough to apply formulas or follow procedures; It is necessary to analyze, evaluate, and solve problems creatively and efficiently. Hands-on activities provide ideal environments to develop and put into practice critical thinking. During practical activities, engineers face real challenges that require careful evaluation of multiple variables and aspects associated with them. This involves questioning assumptions, identifying patterns, and generating innovative solutions to complex problems. Critical thinking manifests itself in the ability to analyze available information, discern between different options, and make informed decisions.

The hands-on activity also encourages collaborative problem-solving. Engineers often work in multidisciplinary teams where each member brings different perspectives and skills. This promotes the exchange of ideas, constructive debate, and the search for comprehensive solutions that contemplate multiple factors and considerations. Furthermore, practical activity in engineering offers the opportunity to experiment with different approaches and techniques. Engineers can test and validate their ideas through prototyping, testing, and simulation, allowing them to learn from their mistakes and continuously improve their skills and knowledge. This iterative process is critical to professional development in engineering and requires constant reflexive thinking to identify areas for improvement and optimization.

B. Statistics in Engineering Practice

Statistics plays a critical role in engineering practices at various levels. First, statistics provides tools for collecting, organizing, and analyzing data in the context of engineering projects. Engineers often face situations where it is required to collect data from experiments, tests, or field studies, and statistics provide them with methods to do so systematically and accurately. In addition, statistics are used to interpret the results of experiments and tests conducted during the development of engineering projects. It allows engineers to determine the reliability and accuracy of the data obtained, identify significant patterns or trends, and make informed decisions based on available information.

Statistics plays a crucial role when designing and analyzing experiments, helping engineers plan data collection efficiently, select representative samples, and determine the appropriate sample size to obtain meaningful and reliable results. In addition, descriptive and inferential statistics are used to model and predict the behavior of complex systems in engineering, allowing engineers a deep understanding of natural phenomena, optimize processes, and make informed decisions about the design and operation of systems and devices. The use of statistics in engineering practices is comprehensive and multifaceted. Also, it provides tools for data collection, analysis, and interpretation, thereby helping to find effective and efficient solutions in a wide range of engineering fields.

III. METHODOLOGY

The simple pendulum experiment was carried out considering different values of thread length, with the same mass, and three oscillations (Fig. 1) [7]. It shows a visual representation of the pendulum used in this engineering practice. This system was made by hand, so the thread used was cotton. The dough was made up of a rubber sphere with a radius of 3.2 cm.

Fig. 1. Visual representation of the simple pendulum.
Source: Generated by recraft AI

The data were analyzed using Excel software, licensed by the University of the Americas. The data were analyzed using Excel software licensed by the University of the Americas. Descriptive statistics were used to treat errors, and theoretical and experimental gravity values were estimated, as well as graphical analysis. In addition to the descriptive statistical analysis performed with Excel software, it is fundamental to highlight the crucial role of graphical visualization tools in engineering data interpretation [8][9]. Visual representation of results through graphs, diagrams, and tables makes it easier to identify trends, anomalies, and relationships between variables, helping engineers better understand the behavior of the systems studied and effectively communicate findings to colleagues, customers, and other stakeholders.

In addition, the use of statistics in engineering is not only limited to the analysis of experimental data but also extends to the design of experiments and process optimization. Engineers can apply advanced statistical techniques, such as factor experiment design or regression analysis, to investigate the influence of multiple variables on a system and identify optimal conditions that maximize performance or minimize costs in the production and operation of engineering systems. Through the strategic use of statistics in all these stages of the engineering process, informed decision-making and continuous improvement are promoted in the search for innovative and efficient solutions.

IV. RESULTS

Table 1 shows the data obtained in the experiment's first phase, showing that triple values have been taken for each length of the pendulum (length of the wire plus radius of the sphere). Additionally, the period values calculated from the number of oscillations are shown.

Table 1. Collected information in the experimental phase.

L(cm)	T1(s)	T2(s)	T3(s)	T^2
13.200	2.050	2.350	2.150	0.530
18.200	2.450	2.450	2.450	0.667
23.200	2.750	2.650	2.750	0.820
28.200	3.050	2.950	3.050	1.011
33.200	3.250	3.450	3.450	1.271
38.200	3.650	3.750	3.550	1.480
43.200	3.950	3.850	3.850	1.675
48.200	3.950	4.050	4.150	1.822
53.200	4.350	4.450	4.250	2.102
58.200	4.550	4.650	4.550	2.334
63.200	4.750	4.750	4.850	2.542
68.200	4.950	4.850	5.050	2.722
73.200	5.250	5.150	5.050	2.946

These data allowed us to estimate the analytical values of gravity, considering the general equation of the pendulum (1)

$$T = 2\pi \sqrt{\frac{l}{g}} \qquad (1)$$

Where T is the period and l is the pendulum's length.

The data obtained in this experimental test are described in Table 2, where gravity values have been grouped and the frequencies have been estimated.

Table 2. Analytical Gravity Results.

g(m/s^2)	f_i
9.81-10.08	6
10.08-10.35	3
10.35-10.62	1
10.62-10.89	1
10.89-11.17	2

The values in the table represent ranges of measurements of acceleration due to gravity (g) in meters per second squared (m/s^2), along with the absolute frequency (f_i) of each range. We observed that most of the measurements (six of them) fall in the range of 9.81 to 10.08 m/s^2, suggesting that this is the most common range of measured values. This could indicate a consistency in measurements within this range, which is crucial for validating the accuracy and reliability of measurements. On the other hand, we noticed that ranges of higher g values have a lower absolute frequency, with only 1 or 2 measurements in each range. This may suggest that these higher values are less common in recorded measurements. These higher values may be associated with measurements made under specific conditions or with less accurate instrumentation, which could require greater attention in terms of calibration and quality control.

The analysis of this table suggests a distribution of g-values, which were centered around the range of 9.81 to 10.08 m/s^2, with some values scattered in higher ranges. This frequency distribution provides useful information about the variability of gravity measurements and can be useful in assessing the accuracy and consistency of the measurements made in the experiment.

Statistical analysis revealed that the mean value of T^2 is about 4.002, and the mean value of acceleration of gravity is about 10.342. On the other hand, the standard deviation for T^2 is around 0.832, and for gravity acceleration, it is about 0.656. The variance for T^2 is about 0.692, and gravity acceleration is about 0.430. We can note an inverse relationship between T^2 and acceleration of gravity, which is consistent with the expected physical relationship between the period of oscillation of a pendulum and the acceleration due to gravity. This is reflected in the negative correlation coefficient of -0.940, indicating a high inverse correlation between these two variables. The data showed that as the period of oscillation squared (T^2) increases, the acceleration due to gravity tends to decrease. This observation agrees with the known physical relationship between these two variables. Which also is observed in the negative correlation coefficient between them. The standard deviation provides a measure of the dispersion of the data around the mean, suggesting that the values of T^2 and gravity acceleration are relatively dispersed.

A. Statistical measures

The statistical data are presented in Table 3. It could be noted that the data do not show the mode. This is because all the values in this category are different.

Table 3. Statistical data.

Stocking	Standard deviation	Variance
2.183	0.153	0.023
2.450	0.000	0.000
2.716	0.058	0.003
3.016	0.058	0.003
3.382	0.115	0.013
3.649	0.100	0.010
3.883	0.058	0.003
4.049	0.100	0.010
4.349	0.100	0.010
4.583	0.058	0.003
4.783	0.058	0.003
4.949	0.100	0.010
5.149	0.100	0.010

Table 4 shows other statistical parameters. It can be noted that the dispersion given by the information is relatively small.

Table 4. Length, time, and gravity dispersion measurements.

	Variance	Standard deviation	Variation range
Lengths(cm)	0.03791666667	0.1947220241	0.6
Time(t)	0.9322089947	0.9655097072	3.2
Gravity (m/s^2)	0.19328	0.4396362132	1.12

The analysis of the simple pendulum is a cornerstone of engineering for several reasons. Due to its simplicity and accuracy, it serves as a fundamental model for understanding a vast array of physical phenomena and dynamical systems. This makes it an invaluable tool for studying concepts like oscillation, simple harmonic motion, and system dynamics. Furthermore, the principles derived from the simple pendulum analysis find application in numerous engineering disciplines. These include the design of structures, optimization of suspension and damping systems, and calibration of measuring instruments. Perhaps most importantly, the simple pendulum's principles are critical for designing control systems that regulate position, speed, and acceleration in mechanical and robotic devices, ensuring their precise and efficient operation.

Moreover, the simple pendulum transcends its role as a theoretical model by enabling the measurement of gravitational acceleration and its variation with both altitude and geographical location. These measurements are crucial in diverse engineering fields, ranging from navigation and geophysics to structural engineering and cartography. This versatility elevates the simple pendulum to a powerful tool in the engineer's toolbox, applicable to understanding core concepts, designing systems and structures, controlling processes, and even performing precise gravity measurements. Its reach extends across numerous engineering disciplines, where it significantly contributes to the development and refinement of innovative and efficient solutions.

CONCLUSIONS

Most acceleration measurements due to gravity (g) fall within the range of 9.81 to 10.08 m/s^2, suggesting consistency in measurements made in this range. This consistency is relevant for validating the accuracy and reliability of measurements, indicating fine quality control in the measurement process. On the other hand, higher acceleration values due to gravity have a lower absolute frequency, suggesting that these values are less common in the measurements made. This may be associated with measurements made under specific conditions or less accurate instrumentation. This finding highlights the importance of calibration and quality control in gravity measurements.

The distribution of gravitational acceleration measurements reveals a clustering around 9.81 to 10.08 m/s^2, with outliers scattered at higher values. This spread offers valuable insights into the measurement variability and can be used to assess the experiment's accuracy and consistency. Furthermore, statistical analysis unveils a robust inverse correlation: as the squared oscillation period (T^2) increases, the measured gravitational acceleration tends to decrease. This aligns perfectly with the expected physical relationship between these variables. This finding deepens our understanding of the link between a pendulum's oscillation period and gravity, potentially leading to new applications in various engineering fields.

These results underscore the critical role of meticulous accuracy and robust quality control in engineering gravity measurements. Consistent measurements within a defined range, contrasted with outliers beyond it, emphasize the necessity of precise instrument calibration and rigorous control of experimental conditions to guarantee reliable data. Furthermore, the robust inverse correlation between the squared oscillation period (T^2) and gravitational acceleration underlines the importance of grasping and accounting for variable interactions in engineering. This finding highlights the power of statistical analysis and mathematical modeling to unveil significant relationships between parameters, offering invaluable insights for design, optimization, and informed decision-making across a broad spectrum of engineering applications.

REFERENCES

[1] J. J. Solaz Portolés & V. Sanjosé López, «El papel del péndulo en la construcción del paradigma newtoniano», vol. 10, Barcelona, 1992, pp. 95-100. 2019.
[2] F. Díaz Céspedes, «El primer experimento de Galileo Galilei,» Letralia, 4 4 2016. [En línea]. Available: https://letralia.com/sala-de-ensayo/2016/04/04/el-primer-experimento-de-galileo-galilei/. [Último acceso: 5 1 2021].
[3] A. Hernández-Fereira. «Ampliación de las posibilidades del sistema hpci-1 para el estudio del movimiento de un péndulo simple real en oscilaciones pequeñas», *Revista Cubana de Física*. Vol. 38, Num. 112. Pp. 112-119. 2021.
[4] R. Espíndola-Heredia & G. del Valle, G. Hernández. «Numerical study of pendulums: From the simple pendulum approximation to the damped physical pendulum with variable mass». *Latin America of Journal Physics Education*. Vol, 2012, vol. 6, no 2, p. 202.
[5] F. M. Fernández. «Perturbation theory in classical mechanics». Europe. *Journal of Physics*. 18, 436. 1997. http://doi.org/10.1088/0143-0807/18/6/005.
[6] A. Zamalloa, G. Cruz, J. Camani, V. Almanza, B. Gonzales, D. Villa & B. Warthon. «Use of Tracker software for teaching distance physics laboratories: Demonstration of error reduction in the simple pendulum». arXiv:2306.06352 [*Physics Education*]. https://doi.org/10.48550/arXiv.2306.06352.
[7] A. Berazain & L.D. Prieto. «¿Cómo impulsar un péndulo? el ejemplo del botafumeiro». *Revista Cubana de Física*. 35, E48. 2018.
[8] G. A. Eguez, D.B. Campuzano, K. M. Katherin & M. T. Velasco. «The pendulum of the hand of statistics and engineering». *Athenea Engineering Sciences Journal*, 4(11), 15-22. 2023.
[9] C. Beainy, E. Caceres, L. Quintero, T. Molina & O. Amezquita. «Instrumento para el aprendizaje del movimiento armónico simple». *South Florida Journal of Development*. 2(1), 839-851. 2021.

ISSN-e: 2737-6419

Athenea Journal
Vol.5, Issue 15, (pp. 16-28)

https://doi.org/10.47460/athenea.v5i15.71

Study of the location for the installation of a photovoltaic plant for the generation of electric power in Puerto Rico

Luz Elena Maldonado Alviarez
https://orcid.org/0009-0009-0246-9957
maldonadoluzelena20@gmail.com
Universidad Simón Bolívar
Programa Doctoral en Desarrollo Sustentable
Caracas-Venezuela

José Luciano Maldonado
https://orcid.org/0009-0004-9001-2917
jlmaldonaj@gmail.com
Universidad de Los Andes
Instituto de Computación y Estadística aplicada
Mérida-Venezuela

Received (26/09/2023), Accepted (15/02/2024)

Abstract. - The description of the geographical location study of a photovoltaic plant to be constructed in the coming years in Puerto Rico is presented as part of a major project the island has embarked upon to enhance its electrical service. This study entailed selecting the terrain based on its topography, as well as assessing the convenience of its location concerning its proximity to the national electrical interconnection system. Additionally, relevant consultations were conducted regarding the rights over the lands that will be affected by the construction of the photovoltaic plant (easements). As a result of this study, a plot of land spanning 131.56 hectares in the Juana Díaz sector, 1.59 kilometers from the electrical interconnected system, was identified as a suitable location, impacting only five easements.

Keywords: photovoltaic plants, renewable energies, sustainable development, global warming.

Estudio de ubicación para la instalación de una planta fotovoltaica para la generación de energía eléctrica en Puerto Rico

Resumen: En este proyecto se realizó un experimento de ingeniería utilizando mediciones para estimar la gravedad analítica y gráficamente. Este enfoque experimental pretende demostrar la utilidad de los principios de ingeniería para verificar los valores de la gravedad terrestre. Se emplearon métodos estadísticos para mejorar la comprensión de los conceptos subyacentes y garantizar una estimación precisa de los errores. Los principales resultados sugieren que esta práctica de ingeniería es una herramienta eficaz para evaluar la gravedad, en la que el análisis estadístico descriptivo desempeña un papel fundamental a la hora de presentar datos fiables y precisos.

Palabras clave: plantas fotovoltaicas, energías renovables, desarrollo sostenible, calentamiento global.

I. INTRODUCTION

A. Climate Change and the Need for Energy Transition

Our planet faces an urgent challenge: reducing uncontrolled greenhouse gas emissions to mitigate global warming. Ensuring a sustainable future for generations to come necessitates immediate action. The energy transition, a shift towards renewable energy sources, is a crucial objective for countries worldwide to lessen the catastrophic impact of climate change. Without concerted efforts to curb environmental pollution, this threat looms large. In this critical context, adopting concrete measures like transitioning to sustainable and renewable energy sources becomes imperative to halt the ongoing rise in global temperatures and safeguard environmental stability. Ultimately, the energy transition is a beacon of hope, guiding countries toward a more sustainable, resilient, and environmentally responsible path.

B. Case Study: Puerto Rico's Renewable Energy Ambitions

This paper presents a case study examining Puerto Rico's ambitious plans for renewable energy integration. The country aims to install and generate 3.750 MW of renewable energy capacity with an additional 1.500 MW of battery storage within the next four years [1][6]-[9]. To achieve this objective, the Puerto Rico Electric Power Authority (PREPA) will issue six Requests for Development Proposals by 2024. Fig. 1 schematically depicts these six tranches, specifying the targeted generation and storage capacity for each phase.

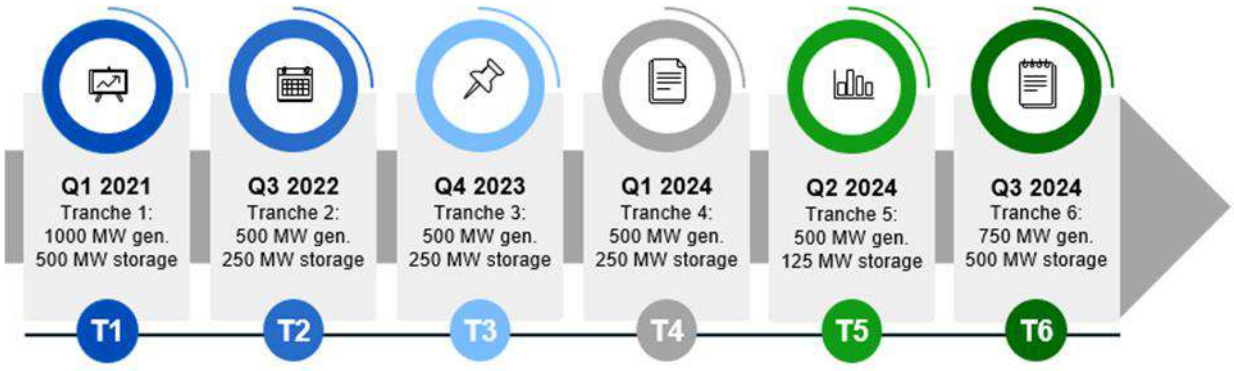

Fig. 1. PREPA Auction Plan involving the 6 tranches
Source: own.

Accion Strategic Energy Group, a Massachusetts-based energy consulting firm with over four decades of experience, has been supporting Puerto Rico's utility industry and government regulators since 2022. The company, along with its island-wide subsidiaries, is currently managing the bidding, review, and award process for Tranche 2, as illustrated in Figure 1. This process aims to select multiple projects that collectively contribute 500 MW of renewable generation and 250 MW of energy storage. Accion established a proposal submission deadline of December 5, 2022. One proposal submitted by Engineering, Procura y Construcción, a Panamanian and Puerto Rican company, focuses on a 25-year Power Purchase Agreement (PPA) to generate 30 MW in the Juana Díaz area. This project entails constructing a 30 MW photovoltaic plant utilizing bifacial panels mounted on fixed structures. Additionally, it includes a 34.5/115 kV step-up substation and a 1.59 km overhead transmission line connecting to the PREPA's TC Canas substation in Ponce (southern Puerto Rico). This paper focuses on the proposed plant's location characteristics.

The paper is structured into the following sections: Introduction, the 30 MW Generation Project for 25 Years, Management of the Photovoltaic Plant, Site Selection for the Photovoltaic Plant, Land Topography, Juana Díaz Land Boundary and Associated Data, Digital Terrain Models (DTMs) of Juana Díaz, Terrain Analysis, Easements and Results Related to the Photovoltaic Plant, and Conclusions.

II. 30 MW GENERATION PROJECT FOR 25 YEARS

This work contributes to a broader effort to establish a comprehensive, 25-year operational management plan for an electric power generation plant in Puerto Rico. Specifically, it details the design and implementation plan for the Juana Díaz 30 MW photovoltaic project. The design process incorporated a sustainability assessment, evaluating the project's environmental, economic, and social impacts. The design plan considered a review of the Puerto Rico Electric System's Administrative Management [3]. Since 1941, the Puerto Rico Electric Power Authority (PREPA) has managed the island's electricity generation, transmission, distribution, and service. The review identified deficiencies in the current system, including infrastructure deterioration, lack of environmental controls, and heavy reliance on fossil fuels (nearly 98%) [3]. Fossil fuel dependence contributes to soil degradation, water pollution, air emissions, and global warming.

On August 24, 2020, the Puerto Rico Energy Bureau issued the Final Resolution and Order on the Integrated Resource Plan of PREPA (Case No. CEPR-AP-2018-0001). This plan mandates the issuance of Requests for Proposals (RFP) tranches to procure renewable energy resources. Tranche 1 seeks at least 3,750 MW of solar PV or other renewables with 1,500 MW of battery storage, while Tranche 2 targets at least 500 MW of solar PV or renewable equivalents with 250 MW of battery storage (1,000 MWh or equivalent) [5]. The proposal described in this article falls under Tranche 2 and focuses on a 25-year Power Purchase Agreement (PPA) to generate 30 MW using photovoltaic technology in the Juana Díaz area [6, 7].

A. Photovoltaic plant management

Table 1 shows, in a general way, the activities involved in the management plan of the photovoltaic plant to be built, from the selection of the land where it will be located, to its design, construction, and commissioning for 25 years.

Table 1. Management activities of the proposed photovoltaic plant.

Nro.	Activity
1	On-site visits and development of topography studies of the selected implantation area.
2	Route from the easements of the 115 kV transmission line to its interconnection to the national energy grid.
3	Proposal for the implementation of the photovoltaic plant with an interconnection route.
4	Installation design of the photovoltaic plant with high-performance equipment.
5	Development of the management plan to manage the project for 25 years.

It's necessary to clarify the scope of this document. This work aimed to contribute to a broader project encompassing the Juana Díaz 30 MW photovoltaic plant. Here, the focus is specifically on the activities related to the land selection process management. Discussions of other project elements, such as plant design and implementation, will be addressed in separate phases of the research.

B. Selection of the site where the photovoltaic plant will be built

Following a comprehensive site analysis considering construction feasibility, the Juana Díaz sector, placed in south-central Puerto Rico, was selected to house the photovoltaic project [6, 7]. This site features irregularly distributed vegetation, including trees and herbaceous plants. Fig. 2. illustrates existing asphalt access roads suitable for transporting materials to the project location and surrounding areas. The land is currently unused for agriculture or livestock, further facilitating project development.

Photographs of the land where the plant will be developed are shown in Fig. 3.

C. Topography of the terrain

To support the initial project management plan, a topographic and photogrammetric survey was conducted in the Juana Díaz field on March 27, 2023. This survey utilized drone technology (specifically, the Mavic 2 Enterprise Advance) integrated with a Geographic Information System (GIS) to generate deliverables including contour lines, digital terrain models (DTMs), high-resolution orthomosaics, property boundaries, and land cover maps [6-9].

Through the Drone technology used, the data services specified in Table 2 were obtained.

Fig. 2. Access roads to the Juana Díaz Terrain.
Source: own.

Fig. 3. Photographs of the Juana Díaz Land where the plant will be developed.
Source: own.

Table 2. Data requested and obtained from the Drone service with their respective formats.

Aerial photographs (.JPG).
Georeferenced image (.GEOTIFF).
Records (.DXF)
3D mesh surface (.PLY and .OBJ)
Orthomosaic map (.JPG, .KLM and .PDF)

Source: own.

The location data of the Juana Díaz land where the photovoltaic plant will be installed and the data obtained from the topographic study are indicated in Tables 3 and 4.

Table 3. Location of the Juana Díaz 30 MW photovoltaic plant, Puerto Rico.

Characteristics of the location of the Photovoltaic Plant	
Municipality	Juana Díaz
Region	Juana Díaz
Country	Puerto Rico
Latitude	+18.05º
Longitude	-66.50º
Altitude	91.14 m a.m.s.l
Time zone	UTC -4

Source: own.

Table 4. Types of Files Obtained from the Topographic Survey.

Images for high-resolution mapping (.JPG).	
Videos (.MP4).	
3D models (.OBJ).	
Records (.DXF), (CAD surveying).	
Elevation models (.PDF, and .KLM)	
NVDI Vegetation Indices (.PDF)	
Orthomosaic	Ortho-mosaic (.JPG, .KLM and .PDF)
Point clouds	.CPR

Source: own.

The files indicated in Table 4 contain all the relevant information on the topography of the land where the plant will be located.

D. Boundaries of land boundaries in Juana Díaz and associated data

The area of interest was delineated using a Keyhole Markup Language (.KML) file [7]. Figure 4 depicts the territorial boundaries of the Juana Díaz sector land parcel.

Fig. 4. Boundaries of the terrain in the Juana Díaz sector.
Source: own.

A total of 4857 cartographic photographs were obtained, captured with a camera at 90 degrees concerning the ground surface in Juana Díaz. That data was acquired on two different trips, according to established flight plans. Figure 5 and Table 5 show the data for the flights executed, which were 155 minutes and 63 minutes respectively.

III. DIGITAL MODELS CREATED FROM THE JUANA DÍAZ TERRAIN

The data acquired digitally allowed the creation of different digital models of the Juana Díaz terrain, which are indicated below:

- **Point Cloud Model:** A model representing the information in the form of a point cloud was created, as shown in Fig. 6. In other words, the digitization of the Juana Díaz terrain made it possible to represent it from a file with 2 million points, showing all the existing, relevant objects on it such as roads, houses, trees, etc.

Fig. 5. Flight Plans in Juana Díaz
Source: own.

Table 5. Topographic survey flight data.

Project	Image Mapping	High Resolution	Low resolution	Flight Height	Area
Juana Díaz	4857	2 cm/px	10 cm/px	262 feet	160ha

Source: own.

Fig. 6. Juana Diaz's Point Cloud.
Source: own.

- **DXF or Contour Line Models:** From a .DXF file you could generate contour line modeling, as shown in Fig. 7, which facilitates the creation of engineering topographic plans for earthworks, slope management, roads, and other facilities. The DXF shows contour lines at a distance of 2 meters, considering that it was not prepared by traditional survey methods using theodolite or total station.

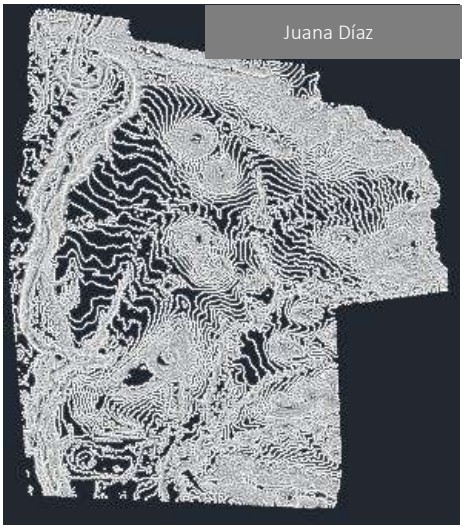

Fig. 7. Contour lines of Juana Díaz
Source: own.

Table 6. Orthomosaic accuracy in meters.

Project	X	And	Z
Juana Díaz	0.8 m	0.9 m	2.6 m

Source: own.

The files that make up the orthomosaic and elevation model are high- and low- resolution images in PDF, KLM, and TIFF formats. Fig. 8 shows the orthomosaics obtained for the project.

Fig. 8. Extension of Juana Díaz's orthomosaic at 10 cm/px.
Source: own.

- **Elevation model:** This model is the layout of a continuous area of the earth's surface, which makes it easier to understand as it represents the slope through a heat map. The accuracy of this data is based on a resolution of 2 cm/px in the high-quality file, while the low-resolution file corresponds to 10 cm/px. These files were obtained in PDF and KLM, both in high and low resolution in TIFF. Figure 9 shows the elevation model obtained for the project.

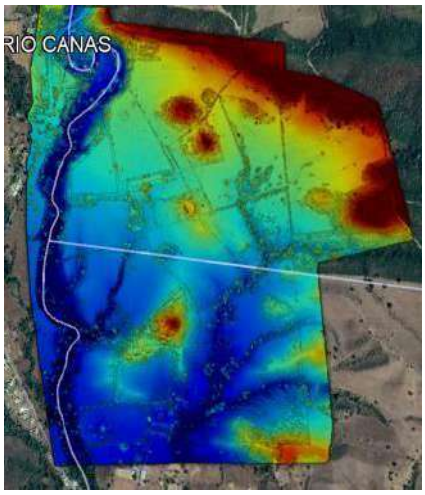

Fig. 9. Juana Díaz Elevation model.
Source: own.

- **OBJ Model:** This model provides three-dimensional (3D) terrain information through the Autodesk Online viewer. From this, data related to the dimensions and heights of the objects can be obtained. Figure 10 shows Juana Díaz's OBJ model.

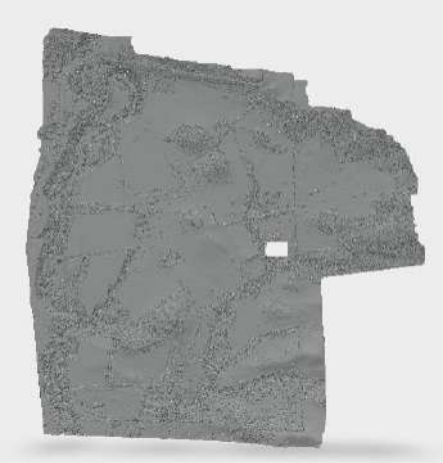

Fig. 10. OBJ Model by Juana Díaz.
Source: own.

- **NVDI Vegetation Model or Index:** Data processing revealed that 62.71 hectares of land in Juana Díaz are suitable for installing the photovoltaic plant, as shown in Figure 12. Digital technology studies confirmed the presence of hills and depressions observed during field visits, thus validating the chosen technology ([6]-[9]). Figure 13 further supports the existence of flat areas within the easement lands.

IV. ANALYSIS OF THE LAND, EASEMENTS AND RESULTS RELATED TO THE PHOTOVOLTAIC PLANT

Data processing revealed that 62.71 hectares of land in Juana Díaz are suitable for installing the photovoltaic plant, as shown in Fig. 12. Digital technology studies confirmed the presence of hills and depressions observed during field visits, thus validating the chosen technology [6]-[9]. Fig. 13 further supports the existence of flat areas within the easement lands.

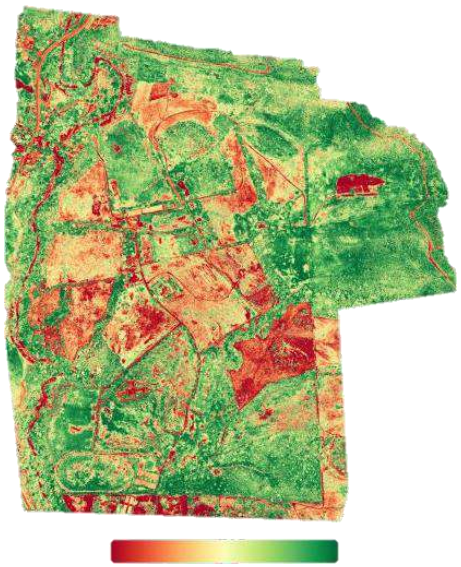

Fig. 11. Image obtained from the NDVI Vegetation Index of Juana Díaz.
Source: own.

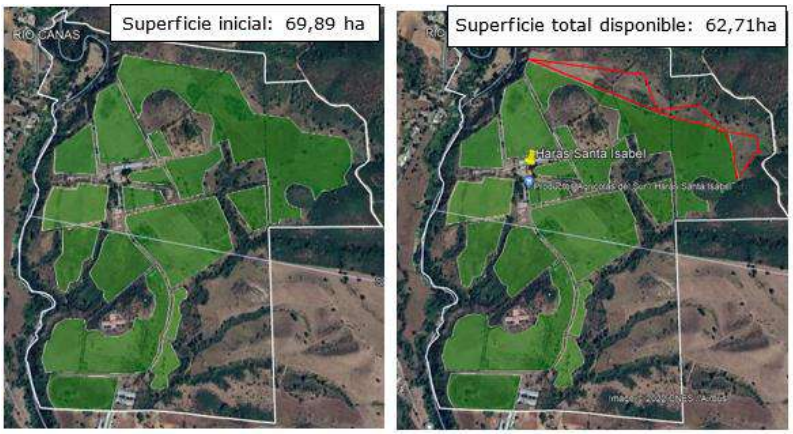

Fig. 12. Comparison of Juana Diaz's total area with the usable area.
Source: own.

The photovoltaic plant will be located on land in Juana Díaz, where the topographic study was carried out, but, additionally, the construction of a 115 kV transmission line that will be interconnected to the principal grid is required. This interconnection is guaranteed since PREPA, in the auction documents, indicates the capacity of its substations to receive energy, as shown in Table 7. It is important to note that most of these substations are located in the south of the island, highlighting a 115 kV transmission line coming from the TC Cañas substation, as shown in Table 7, which is the line to which the 30 MW Juana Díaz photovoltaic project will be interconnected, as described in this article, through a disconnecting switch using the "Breaker and a half" design, at the site shown in Fig. 14.

Fig. 13. Juana Díaz Land Easement.
Source: own.

Table 7. Available Capacity in Substations for Interconnection Renewable Energy Plants in Puerto Rico.

POI Station-Existing	POI Voltage (kV)	Maximum Size MW Solar PV Injection	Maximum Size MW Storage	Latitude	Longitude
Maunabo TC	38	10		18.0115	-65.9043
Veredas Sect.	38	10		18.2249	-66.0074
Manati Sect.	38	10		18.4424	-66.6378
Jobos TC	115	50		17.9615	-66.1395
CT Gray Hair	115	100	100	18.0128	-66.6392
Santa Isabel TC	38	10		18.022	-66.3697
Santa Isabel TC	115	10		18.022	-66.3697
Juana Díaz TC	115	150		18.0598	-66.5513

Source: PREPA.

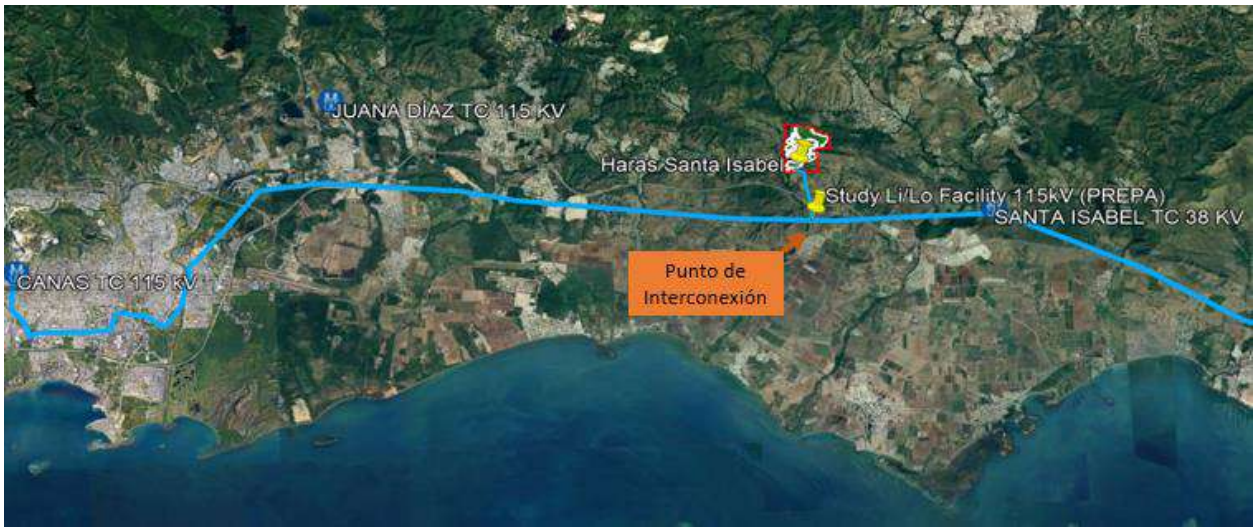

Fig. 14. Transmission Line where the interconnection will be made.
Source: own.

Fig. 15 shows in detail the most efficient route, from a technical and economic point of view, between the Juana Díaz land and the Point of Interconnection (POI) through a 1.59 km 115 kV transmission line.

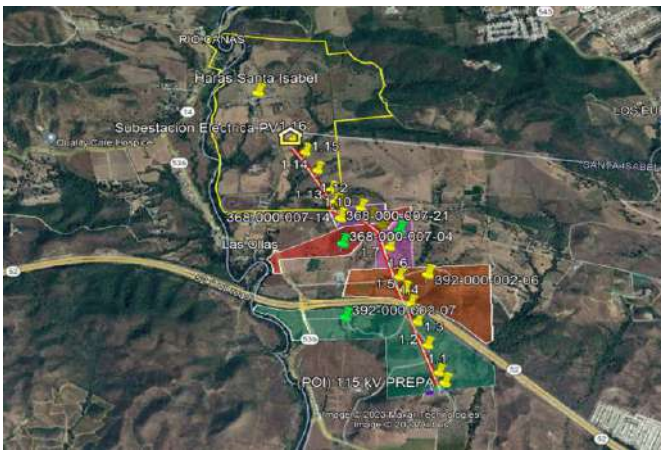

Fig. 15. Route of the 115 kV transmission line from the Juana Díaz land to the point of interconnection.
Source: own.

As can be seen in the image in Fig. 15, the transmission line will pass through five plots of land. These five lots are identified because they correspond to different owners, which were located through the CRIM (Municipal Tax Collection Center). The five affected easements are shown in Table 8.

Table 8. Number of easement parcel data on the 115 kV transmission.

Item	Parcel Number According to CRIM	Route of Power Line in Easements (m)	Surface Line Easement Area (Ha)
1	368-000-008-15	398	0.89
2	368-000-007-24	107	0.26
3	368-000-007-22	620	0.96
4	392-000-012-16	485	0.86
5	392-000-012-27	830	2.12
115 kV Power Line Easements		**2440.00**	**5.09**

Source: own.

Table 4 shows other statistical parameters. It can be noted that the dispersion given by the information is relatively small.

In these designated easements, transmission towers will be erected to support the overhead transmission line, measuring approximately 30 meters in height and 16 meters in width, until reaching the interconnection site where the interconnection disconnector will be additionally constructed.

The specific impacts on the easement lands are outlined as follows:

- **Easement 1**, 368-000-008-15: This easement necessitates the installation of 2 transmission towers.
- **Easement 2**, 368-000-007-24: Within easement 368-000-007-24. The installation of one transmission tower is mandated.
- **Easement 3**, 368-000-007-22: For easement 392-000-012-27, the installation of one transmission tower is required.
- **Easement 4**, 392-000-012-16: In easement 4, identified as 392-000-012-16, the installation of 1 transmission tower is needed.
- **Easement 5**, 392-000-012-27: Within easement 392-000-012-27, the installation of 4 transmission towers and a disconnector is necessary for grid interconnection.

CONCLUSIONS

In this study aimed at determining an optimal site for the proposed photovoltaic project, it was identified that the most suitable location is a parcel of land within the Juana Díaz sector, situated in the south-central region of Puerto Rico. This selection was made based on several key factors: the presence of tree and herbaceous vegetation, albeit not in abundance; the sufficiently flat terrain; the presence of asphalt roads providing access to surrounding lands and farms; and its proximity, at a distance of 1.59 km, to the interconnection point of the national electricity system.

Moreover, during the project's execution, only five plots of land, owned by different individuals, will be affected. Agreements were successfully negotiated with these landowners without encountering significant obstacles. The proposal for the Photovoltaic Plant's development on the identified land underwent rigorous review by PREPA, ultimately receiving approval. This endorsement not only validates the suitability of the chosen location but also underscores its potential to contribute significantly to Puerto Rico's energy supply over the next twenty-five years.

The decision to select Juana Díaz as the site for the photovoltaic plant was informed by a comprehensive assessment that considered not only topographical and logistical factors but also prioritized effective collaboration with local landowners. The presence of vegetation, coupled with the flat terrain, suggests a balanced ecological environment that will minimize the project's environmental footprint. Accessible infrastructure, including asphalt roads, ensures seamless logistics during both the construction and operation phases.

The cooperative agreements with affected landowners demonstrate a proactive approach to managing easements, reflecting a positive synergy between project development and community interests. This collaborative spirit, coupled with PREPA's approval, underscores the strategic significance of Juana Díaz as a model for sustainable development that harmonizes technical, environmental, and social considerations, promising both increased energy capacity and long-term sustainability for Puerto Rico.

REFERENCES

[1] N. Singh. (2022). Así es el plan de Puerto Rico para impulsar 3700 MW renovables junto a almacenamiento [Online]. Available: https://www.energiaestrategica.com/asi-es-el-plan-de-puerto-rico-para-impulsar-3700-mw-renovables-junto-a-almacenamiento/

[2] N. Singh. (2022). Panorama 2022: Estas son las licitaciones de energía activas, interrumpidas y pendientes en Latinoamérica [Online]. Available: https://www.energiaestrategica.com/panorama-2022-licitaciones-de-energia-activas-interrumpidas-y-pendientes-en-latinoamerica/

[3] S. Caraballo. (2019). Comentarios sobre la nueva política pública y el marco regulatorio del sistema eléctrico de Puerto Rico. Revista Jurídica UPRRP [Online]. Available: https://derecho.uprrp.edu/inrev/2019/01/31/comentarios-sobre-la-nueva-politica-publica-y-marco-regulatorio-del-sistema-electrico-de-puerto-rico/

[4] Ley Núm. 120 de 20 de junio de 2018. (2018). Ley para transformar el sistema eléctrico de Puerto Rico [Online]. Available: https://energia.pr.gov/wp-content/uploads/sites/7/2019/05/120-2018.pdf

[5] Government of Puerto Rico Public Service Regulatory Board Puerto Rico Energy Bureau. (2022). Motion to reiterate the request for entry of resolution and order detailing PREPA's role in the Tranche 2 RFP process [Online]. Available: https://energia.pr.gov/wp-content/uploads/sites/7/2022/01/Motion-to-Reiterate-Request-For-Entry-Of-Resolution-And-Order-Detailing-PREPAs-Role-In-The-Tranche-2-RFP-Process-NEPR-MI-2020-0012.pdf

[6] Acama Solar. (2011). Declaración de Impacto Ambiental: Proyecto Parque Fotovoltaico Atacama Solar 250 MW [Online]. Available: https://www.caf.com/media/6752/declaracion-de-impacto-ambiental-dia.pdf

[7] Aresol Energías Renovables. (2020). PROYECTO DE PARQUE SOLAR FOTOVOLTAICO "JUMILLA" DE 9.74MWp EN JUMILLA (MURCIA) [Online]. Available: https://transparencia.carm.es/wres/transparencia/doc/Infoub/4E20ATE007264_PSFV_PROYECTO_PARQUE_SOLAR_JUMILLA.pdf

[8] Solar Power Europe. (2023). Global Market Outlook: For solar power 2023-2027. Focus on Southeast Asia [Online]. Available: https://gycxsolar.com/wp-content/uploads/2023/10/GYCX-SolarsolarPower_Europe_GlobalMarketOutlook_for_SolarPower_2023-2027.pdf

[9] Engr.dcet. (2023). Solar Power Plant Construction and Working. [Online]. Available: https://paktechpoint.com/solar-power-plant-construction-and-working-pdf/

ISSN-e: 2737-6419

Athenea Journal
Vol.5, Issue 15, (pp. 29-40)

https://doi.org/10.47460/athenea.v5i15.72

Novel Methodology for Characterization of Thermoelectric Modules and Materials

Pirela Ronald
https://orcid.org/0000-0002-1411-6333
repirelalc@estudiante.unexpo.edu.ve
IEEE Membership
Savigliano-Italia

Velásquez Sergio
https://orcid.org/0000-0002-3516-4430
svelasquez@unexpo.edu.ve
Universidad Experimental Politécnica
Antonio José de Sucre
Puerto Ordaz-Venezuela

Received (30/10/2023), Accepted (25/02/2024)

Abstract. - The document presents an innovative methodology that combines forced response and natural response theories in thermoelectric materials and devices. It stands out for expressing the thermoelectric figure of merit in terms of the ratio of two temperatures $Z\bar{T} = \Delta T'/\Delta T$, enabling comprehensive testing and precise characterization of thermoelectric modules and materials, including measurements of thermal conductance, electrical resistance, Seebeck coefficient, and figure of merit. Additionally, it addresses the determination of thermal resistances and thermal capacitances related to thermal contacts, as well as the derivation of characteristic time constants and angular frequencies. This approach, applicable to both modular devices and individual samples, allows for the simultaneous measurement of all parameters on a single sample. The experiments considered non-ideal contacts and non-adiabatic conditions at room temperature $\bar{T} = 300K$, enhancing the feasibility of in-situ characterization and positioning this methodology as a key tool in thermoelectric research.

Keywords: thermoelectric characterization, Harman method, transient test method, thermoelectric time constants, thermoelectric frequencies, complete response, figure of merit.

Metodología novedosa para la caracterización de módulos y materiales termoeléctricos

Resumen: El documento presenta una metodología innovadora que combina teorías de respuesta forzada y respuesta natural en materiales y dispositivos termoeléctricos. Destaca por expresar la figura de mérito termoeléctrica en términos de la relación de dos temperaturas $Z\bar{T} = \Delta T'/\Delta T$, permitiendo ensayos completos y caracterizaciones precisas de módulos y materiales termoeléctricos, incluyendo mediciones de conductancia térmica, resistencia eléctrica, coeficiente de Seebeck y figura de mérito. Además, aborda la obtención de resistencias térmicas y capacitancias térmicas relacionadas con contactos térmicos, así como la determinación de constantes de tiempo características y frecuencias angulares. Este enfoque, aplicable tanto a dispositivos modulares como a muestras individuales, posibilita la medición simultánea de todos los parámetros en una misma muestra. Los experimentos consideraron contactos no ideales y condiciones no adiabáticas a temperatura ambiente \bar{T}=300K mejorando la viabilidad de la caracterización in situ y posicionando esta metodología como una herramienta clave en la investigación termoeléctrica.

Palabras clave: caracterización termoeléctrica, método de Harman, método de prueba transitorio, constantes de tiempo termoeléctricas, frecuencias angulares termoeléctricas, figura de mérito.

I. INTRODUCTION

The Thermoelectric Modules and Thermoelectric Materials (TEMs) are solid-state power converters that typically consist of p and n type semiconductor material arrangements, connected so that they are thermally in parallel and electrically in series [1] [2] [3] [4]. TEMs are marketed for applications in the areas of cooling and heating; as well as for the generation of electrical power, collecting solar energy and residual heat [5] [6]. One of the arduous tasks that must be carried out in the thermoelectric field is the characterization of thermoelectric materials and modules [7]. It is essential to obtain reliable measurements of global efficiency to assess its technological and economic interest [8] [9]. Another challenge to meet is to determine the performance of thermoelectric devices adequately and accurately [10]. The thermoelectric performance is reduced to the determination of a single quantity called the figure of merit $Z\bar{T}$ and a way of expressing it is presented in (1), where $\bar{T}$ is the average working temperature of the system, R_m is the electrical resistance of the module, K_0 is the thermal conductance to the vanishing electric current, and α is the global Seebeck coefficient characterizing the thermoelectric coupling between the electric current and the heat flux through the TEM terminals. The figure of merit $Z\bar{T}$ is related to the theoretical maximum efficiency of a thermoelectric generator that works between two thermal reservoirs, one at a hot temperature T_h and the other at a cold temperature T_c, where $T_c < T_h$. The maximum efficiency η_{max} is determined by means of (2), in which $\eta_C = 1 - T_c/T_h$ is the Carnot efficiency [11] [12].

$$Z\bar{T} = \frac{\alpha^2 \bar{T}}{R_m K_0} \tag{1}$$

$$\eta_{max} = \eta_C \frac{\sqrt{1 + Z\bar{T}} - 1}{\sqrt{1 + Z\bar{T}} + T_c/T_h} \tag{2}$$

The precise evaluation of $Z\bar{T}$ is far from simple, and several approaches can be applied, e.g.: measure α, K_0 y R_m separately and then calculate $Z\bar{T}$ using (1). However, this method is quite inaccurate without great experimental attention, since each measurement error for each parameter contributes to the accumulated global error in the resulting $Z\bar{T}$ value [13] [14]. Other methods use different measurement systems for each property. Often the three main properties are not measured on the same sample or in the same direction. Also, these methods are time-consuming and susceptible to increasing the uncertainties in $Z\bar{T}$. In the late 1950's a method was presented by Harman for testing the resistance in alternating current and determining the figure of merit of a thermoelectric material sample [15]. Also, the same methodology was used by Harman, Cahn, and Logan for the measurement of thermal conductivity applying the Peltier Effect [16]. This technique has many variations and it has been traditionally applied to both bulk modules and thin films. The drawbacks are that it only works with small temperature differences and requires adiabatic boundary conditions that can be difficult to satisfy [17] [18]. In the early 1990s a test methodology was developed by Buist, this method is referred to as the transient test method [19], which is based on a similar concept but some fundamental differences compared with Harman's method which gave rise to improvement in accuracy, and reproducibility [5] [20]. The fundamental similarity is that the two techniques cited above are designed to solve the voltage components of a thermoelectric device and the fundamental difference is that the Harman method does this by measuring the resistive component and the transient test method measures the Seebeck component, whereas the novel methodology for characterization hat this moment described is designed by determination of the thermal components, and it is intended to provide the ultimate solution for measuring the thermal conductance, thermal conductivity and the figure of merit of TEMs.

The new method presented in this paper provides a set of guidelines for the direct measurement of all the parameters needed to characterize the thermoelectric properties of either materials and devices under test, such as the thermoelectric resistance of the module R_{TE}, thermal resistances related to thermal contacts R_C, thermoelectric capacitance of the module C_{TE}, thermal capacitances related to thermal contacts C_C, thermal resistance of the thermoelectric material R_0 and the capacitance of the thermoelectric material C_{th}. As well the Seebeck coefficient α, electrical resistance R_m, thermal conductance K_0, electrical resistivity ρ, thermal conductivity κ and figure of merit $Z\bar{T}$. Additionally, through this methodology is possible to determine the characteristic time constants and relaxation times, as well as the characteristic angular frequencies.

This article is structured as follows: in section II the complete response of TEMs is presented, then in section III the temperature and voltage stability are explained, obtaining as a result the characteristic thermoelectric time constants τ_{TE}, τ_{th}, τ_C and the relaxation times, and it continues to section IV developing thermoelectric modeling and equation derivations, where new equations of the figure of merit $Z\bar{T}$ are shown in V characterization configurations. Finally, the experimental results, implementation, conclusions, and references. Furthermore, this research is framed within UNESCO's 2015-2030 agenda for sustainable development, specifically objective number 7, entitled “Affordable and Clean Energy”, which aims to improve access to clean energy through inclusive science, technology, and innovation systems (STI).

II. COMPLETE RESPONSE OF THERMOELECTRIC MODULES AND MATERIALS

The temperature difference and voltage of TEMs generated due to the Peltier and Seebeck effects, respectively [2] [1], have two components and there are two classical ways to break it down into two parts. The first way is to divide it into “a forced response (independent source) and a natural response (stored energy)”, and the second way is to divide it into “a steady-state response (permanent or stable part, this is the behavior of the TEMs long after external excitation applied) and a transient response (temporary part, which will extinguish with time)” [20].

The unification of the forced response (slow and fast perturbation) and natural response (absence of perturbation) theories allows for a description of the complete response of thermoelectric modules and materials; as well as allows the study and characterization of TEMs [21] [22] [23]. The equations used to represent the complete response (or total response) of a thermoelectric module either to the abrupt application of a DC voltage source on the electrical terminals or to the abrupt application of a temperature differential on the thermal contacts are shown in (3) and (4), respectively; assuming that the thermoelectric module represents a thermoelectric capacitor initially discharged and at $t = 0$, $\Delta T(0) = 0$, and $V_\alpha(0) = 0$.

$$\Delta T(t) = \alpha \bar{T} I R_{TE} + [\Delta T(0) - \alpha \bar{T} I R_{TE}] e^{-t/\tau_{TE}} \quad (3)$$

$$V_\alpha(t) = \alpha \Delta T + [V_\alpha(0) - \alpha \Delta T] e^{-t/\tau_{TE}} \quad (4)$$

A. Forced response of thermoelectric modules and materials

The forced response of TEMs can be obtained through the temperature difference or the voltage generated by a TEM, from the corresponding Peltier and Seebeck effects, and are given by the mathematical expressions (5) and (6) [22]. Where $\Delta T(t)$ is the temperature difference measured across the thermal contacts of the TEM, α is the Seebeck coefficient, $\bar{T}$ is the average temperature, R_{TE} is the thermoelectric resistance, I is the electric current. Also, $\Delta T(t) = T_h(t) - T_c(t)$, $\alpha = V_\alpha/\Delta T$ and $I = [V_s u(t) + V_\alpha(t)]/R_m$, in which $V_s u(t)$ represents the external voltage source, $V_\alpha(t)$ the Seebeck voltage, R_m the electrical resistance of the TEM. And τ_{TE} is the thermoelectric time constant of the module.

$$\Delta T(t) = \alpha \bar{T} I R_{TE}\left(1 - e^{-t/\tau_{TE}}\right) \quad (5)$$
$$V_\alpha(t) = \alpha \Delta T\left(1 - e^{-t/\tau_{TE}}\right) \quad (6)$$

Consequently, for the case where the thermal contacts are absent; i.e., the case where there is only the presence of thermoelectric material, mathematical expressions (5) and (6) are reduced to expressions (7) and (8), where $\Delta T'$ is the temperature differential generated at the thermal terminals by the thermoelectric material, R_0 is the thermal resistivity of the thermoelectric material and τ_{th} is the characteristic thermoelectric time constant of the thermoelectric material.

$$\Delta T'(t) = \alpha' \bar{T} I R_0\left(1 - e^{-t/\tau_{th}}\right) \quad (7)$$
$$V'_\alpha(t) = \alpha' \Delta T'\left(1 - e^{-t/\tau_{th}}\right) \quad (8)$$

It should be noted that the forced response of TEMs expressed in the temperature difference is the exponential increase of the Peltier effect and expressed in voltage is an exponential increase of the Seebeck effect and complies with the theory of first-order electrical circuits [22].

B. Natural response of thermoelectric modules and materials

Since the theory of the natural response of TEMs, it is known that the temperature difference associated with the thermoelectric capacitance of the thermoelectric material is $\Delta T_{C_{th}}$ and is defined as $\Delta T_{C_{th}} = \Delta T' = T_{hM} - T_{cM}$ and the temperature difference related to the equivalent thermal capacitance of the thermal contacts is given by ΔT_{C_C}. Thus, the natural response of a thermoelectric module is defined by equations (9) and (10) [23].

$$\Delta T = \Delta T' + \Delta T_{C_C} \quad (9)$$
$$V_\alpha = \alpha\left[\Delta T' + \Delta T_{C_C}\right] \quad (10)$$

The formal mathematical expression for ΔT_{C_C} is presented in (11).

$$\Delta T_{C_C} = A_1 e^{s_1 t} + A_2 e^{s_2 t} \quad (11)$$

Where, $s_1 = -\beta + \sqrt{\beta^2 - {\omega_0}^2}$ and $s_2 = -\beta - \sqrt{\beta^2 - {\omega_0}^2}$ are the roots and are called natural frequencies, measured in Nepers per second (Np/s), because they are associated with the natural response of the thermoelectric device; ω_o is called the resonant frequency of the thermoelectric module, or more strictly the undamped natural frequency of the TEM, expressed in radians per second (rad/s), and β is the natural frequency or damping factor, expressed in Nepers per second, and represents the frequency associated with the thermal contacts and is also called ω_1, therefore $\beta = \omega_1$. Further, considering that at $t = 0$, $A_1 = \alpha \bar{T} I_{TEG_{sc}} R_{c_{cold}}$ and $A_2 = \alpha \bar{T} I_{TEG_{sc}} R_{c_{hot}}$, where $R_{c_{cold}}$ is the thermal resistance of the contact cold side of the TEM, $R_{c_{hot}}$ is the thermal contact resistance of the hot side of the TEM, and $I_{TEG_{sc}}$ is the short-circuit current of the device in thermo generator mode; that is, the load R_{Load} connected to the thermogenerator is zero ohms. So, for $R_{Load} = 0$, we have that $I_{TEG_{sc}} = V_\alpha / R_m$. And the formal mathematical expression for $\Delta T'(t)$ is as shown in (12).

$$\Delta T'(t) = A_1 e^{-\beta_{th} t} \cos \omega_d t + A_2 e^{-\beta_{th} t} \text{sen}\, \omega_d t \quad (12)$$

Therefore, the natural response concerning the thermoelectric material is defined using the following expressions (13) and (14).

$$\Delta T'(t) = e^{-\beta_{th} t}(A_1 \cos \omega_d t + A_2 \text{sen}\, \omega_d t) \quad (13)$$
$$V'_\alpha(t) = \alpha'\left[e^{-\beta_{th} t}(A_1 \cos \omega_d t + A_2 \text{sen}\, \omega_d t)\right] \quad (14)$$

The time constant associated with the capacitance of the thermoelectric material τ_{th} could be obtained at a slightly longer time than expected. Considering that the amplitude is reduced by a factor $1/e$ (to 36.8 % of what it had), it can be achieved at a longer time to the relation $\tau_{th} = 1/\omega_{th}$, where ω_{th} is the characteristic angular frequency related to the thermoelectric material, for which the case of an overdamped thermoelectric circuit is considered when $\beta < \omega_0$. Therefore, the roots can be write as $s_1 = -\beta + \sqrt{-(\omega_0{}^2 - \beta^2)} = -\beta + j\omega_d$, and $s_2 = -\beta - \sqrt{-(\omega_0{}^2 - \beta^2)} = -\beta - j\omega_d$, where $j = \sqrt{-1}$ and $\omega_d = \sqrt{(\omega_0{}^2 - \beta^2)}$ is called the damping frequency. Both ω_0 and ω_d are natural frequencies, because they help determine the natural response of the TEM; while ω_o is often called the undamped natural frequency, ω_d is called the damped natural frequency or offset frequency. Such a response has a time constant associated with the thermoelectric capacitance τ_{th} and a period of $T = 2\pi/\omega_d$, and as the amplitude is reduced by a factor $1/e$ (to 36.8 % of what it had), we then have two scales of time: T measures the time it takes to oscillate and τ_{th} the time it takes to damp. The dimensionless quotient is represented in (15) [23].

$$\frac{\tau_{th}}{T} = \frac{\omega_d}{2\pi\beta_{th}} \tag{15}$$

It is important to highlight that the natural response of TEMs expressed in temperature is an exponential drop in the temperature difference and satisfies the Newton's law of cooling, and the natural response of TEMs expressed in voltage is an exponential Seebeck voltage drop and complies with second order electrical circuits theory [23].

C. Temperature and voltage stability

The thermoelectric time constant τ_{TE} is obtained from the forced response (step response) of TEMs, from the temperature difference $\Delta T(t)$ on the faces of the module (Peltier effect), from the temperatures of either any of the thermal contacts $T_c(t)$, $T_h(t)$ or electric potencial $V_\alpha(t)$ generated between the positive and negative terminals of the TEMs (Seebeck effect) [22]. The time constant τ_{TE}, corresponds to the inverse of the characteristic thermoelectric angular frequency of the TEMs $\tau_{TE} = 1/\omega_{TE}$ and is the time required for $\Delta T(t)$, $T_c(t)$, $T_h(t)$ y $V_\alpha(t)$ to increase by a factor of "e" or 63.2% of its final value; that is, they take $5\tau_{TE}$ to reach their steady state, when no change occurs over time [22]. Taking into account that, $\tau_{TE} = C_{TE}R_{TE}$.

The time constant associated with the capacitance of the thermal contacts τ_C is obtained from the natural response of the TEMs, specifically from the temperature of the thermal contact related to the cold side [23]. For the case where the thermal contact of the cold side is equal to the thermal contact of the hot side, the time constant τ_C is obtained experimentally from the temperature measurement on the face of the cold side of the device T_c and is determined considering that the amplitude is increased by a factor $1/e$ (36.8 % of the amplitude that it would have), so $\tau_C = 1/\beta = 1/\omega_1$, where $\tau_C = C_C R_C$. The damping factor β determines the rate at which the response is damped. The time it takes for the temperature of the cold side to rise is given by the decay of factor β. So the thermal capacitor will be fully discharged after five time constants. In other words, the capacitor associated with the thermal contact on the cold side of the TEM takes $5\tau_C$ to reach its final state [23].

The thermoelectric time constant related to the thermoelectric material τ_{th} is also obtained from the natural response. From equation (15) an expression is obtained for the characteristic angular frequency related to the thermoelectric material which is known as ω_{th}, and is given by the following mathematical expression in (16).

$$\omega_{th} = 2\pi\beta_{th} = \frac{2\pi}{\tau_{th}} \tag{16}$$

The time that takes the amplitude of the temperature difference between the faces of the TEMs (either ΔT or $\Delta T'$) to decay is given by the time constant $\tau_{th} = C_{th}R_0$ is obtained through the following equation (17) [23].

D. Thermoelectric modeling and equation derivation

Thermoelectric coefficients and parameters *of TEMs*

Using the theory of forced response, it is possible to obtain the thermoelectric resistance R_{TE}, using (5) [22]. Considering that, for the forced response, at $t = 0$, the temperature difference $\Delta T(0) = 0$ and that after $5\tau_{TE}$ it will reach its steady state, then $R_{TE} = \Delta T(t)/\left[\alpha\bar{T}I\left(1 - e^{-t/\tau_{TE}}\right)\right]$, and it can be expressed in a more compact way if it is taken into consideration that for a time greater than $t > 5\tau_{TE}$, $e^{-t/\tau_{TE}}$ tends to zero, then an expression for R_{TE} is shown in (18).

$$R_{TE} = \frac{\Delta T}{\alpha\bar{T}I} \tag{18}$$

Using the theory of natural response, the equivalent resistance of the thermal contacts is obtained R_C and is found through (11) [23]. Equation (11) shows that ΔT_{C_C} is the result of the temperature contribution of each thermal contact and R_C is the result of the sum of the thermal resistances of the thermal contacts. Assuming that the thermal resistances corresponding to the contacts are equal, $R_{c_{cold}} = R_{c_{hot}}$, that the equivalent resistance of the contacts is $R_C = R_{c_{cold}} + R_{c_{hot}}$ and $A_1 = A_2$, then $\Delta T_{C_C}(t) = \alpha\bar{T}I_{TEG_{sc}}R_C e^{s_1 t}$. Taking into account that, at $t = 0$, the maximum value of ΔT_{C_C} is obtained. Additionally, that $V_\alpha = \alpha\Delta T$ and $I_{TEG_{sc}} = V_\alpha/R_m$, so $I_{TEG_{sc}} = \alpha\Delta T/R_m$. Therefore, the thermal resistance related to thermal contacts can be written as in (19) [22] [23]. The electric resistance of TEMs R_m is found using (20) [3] [4]. And, to find the electric resistivity ρ it is recommended to use the equation (22), which correlates R_m and the geometry of the specimen under test.

$$R_C = \frac{R_m \Delta T_{C_C}}{\alpha^2 \bar{T}\Delta T} \tag{19}$$

$$R_m = \frac{V_{max}}{I_{max}} \frac{(T_h - \Delta T_{max})}{T_h} \tag{20}$$

Also, using the theory of natural response, the thermal conductance K_0 is obtained, considering the equation (12). With the presence of the sine and cosine functions it is trivial that the natural response for this case is exponentially damped and oscillatory in nature. Considering that, at $t = 0$ the maximum value of the temperature difference $\Delta T'$; also that $A_1 = A_2 = \alpha\bar{T}I_{TEG_{sc}}R_0$, $\operatorname{sen}\omega_d t = 0$ and $\cos\omega_d t = 1$; that is, a term in (12) contributes neither to the temperature difference $\Delta T'(t)$ nor to the Seebeck voltage $V_\alpha(t)$. Therefore, the thermal resistance of the thermoelectric material is $R_0 = \Delta T'/\alpha\bar{T}I_{TEG_{sc}}$ and knowing that the thermal conductance is equal to the inverse of the thermal resistance; that is, $K_0 = 1/R_0$, then the thermal conductance of the thermometric material is given by $K_0 = \alpha\bar{T}I_{TEG_{sc}}/\Delta T'$. Hence, the thermal conductance of the thermoelectric material can be written as in (21), keeping in mind that $I_{TEG_{sc}} = \alpha\Delta T/R_m$. Furthermore, from the forced response is possible to find that $K_0 = (1/R_{TE}) - (1/R_C)$.

$$K_0 = \frac{\alpha^2\bar{T}\Delta T}{R_m \Delta T'} \tag{21}$$

The electric resistivity is obtained using (20) by multiplying R_m per A/L, where L and A are the length and area of the specimen under test, obtaining the equation (22). Also, the thermal conductivity of the thermoelectric material κ is obtained through (21) by multiplying K_0 per L/A, obtaining the equation (23).

$$\rho = \left[\frac{V_{max}}{I_{max}} \frac{(T_h - \Delta T_{max})}{T_h}\right]\left(\frac{A}{L}\right) \tag{22}$$

$$\kappa = \left(\frac{\alpha^2\bar{T}\Delta T}{R_m \Delta T'}\right)\left(\frac{L}{A}\right) \tag{23}$$

Figure of Merit

As it is known, the figure of merit is calculated using (1). However, by substituting (21) into (1), a new expression is found for the figure of merit and is written utilizing the mathematical equation (24).

$$Z\bar{T} = \frac{\alpha^2 \bar{T}}{R_m K_0} = \frac{\Delta T'}{\Delta T} \tag{24}$$

Solving $\Delta T'$ from equation (9) it is found that $|\Delta T'| = \left|\Delta T - \Delta T_{C_C}\right|$ and substituting into (24) is obtained (25). Since $\left|\Delta T_{C_C}\right|$ is the result of the temperature contribution of each thermal contact, $T_{C_{hot}}$ and $T_{C_{cold}}$, where $T_{C_{cold}} = T_c$(℃) and $T_{C_{hot}} = T_h$(℃), more expressions are found as shown in (26), (27), (28), and (29).

$$Z\bar{T} = \frac{\Delta T - \Delta T_{C_C}}{\Delta T} \tag{25}$$

$$Z\bar{T}_{TEC} = \frac{\Delta T - T_c}{\Delta T} \tag{26}$$

$$Z\bar{T}_{TEG} = \frac{\Delta T - T_h}{\Delta T} \tag{27}$$

$$Z\bar{T}_{TEC} = 1 - \frac{T_c}{T_h - T_c} \tag{28}$$

$$Z\bar{T}_{TEG} = 1 - \frac{T_h}{T_h - T_c} \tag{29}$$

The new expression for the figure of merit of TEM obtained in this research; e.g., $Z\bar{T} = \Delta T'/\Delta T$ has the form of the Harman equation $Z\bar{T} = V_\alpha/V_p$, but the $Z\bar{T}$ equation obtained herein is expressed as a function of temperatures and the one obtained by T. C. Harman is expressed as a function of voltages [15]. Equations (25), (26), and (27) for the figure of merit reciprocally have the form of the equation $Z\bar{T} = V_{oa}/(V_{ia} - V_{oa})$, obtained by R. Buist [19]. Furthermore, the second term on the right-hand side of equation (28) corresponds to the expression obtained by A. F. Ioffe [12], to measure the maximum performance ϵ_{max} of the TEM; that is, $\epsilon_{max} = T_1/(T_0 - T_1)$, where $T_1 = T_c$ and $T_0 = T_h$.

III. CHARACTERIZATION CONFIGURATIONS

A. Test Configuration for Thermoelectric Modules

Through Figure 1 (a), four different test configurations for a thermoelectric module are illustrated. The "*Suspended*" configuration employs the four probes test technique. The method used to adhere the thermocouples to the thermal contacts is simply to apply a tiny dab of thermal paste where the thermocouple junctions are positioned and can be held in place under compression with the use of thermal insulation tape [5] [19]. The "*Suspended*", "*Heat Sink*" and "Assembly" configurations are essentially the same because these configurations employ the four probes test technique. The "*Thermocouples*" configuration provides the ultimate solution in simplicity, connections, and speed of testing. This configuration is especially recommended when TEMs are used as thermogenerators. The main parameter measured using this setup is $Z\bar{T}$. This is enough to ensure the production quality of thermoelectric modules.

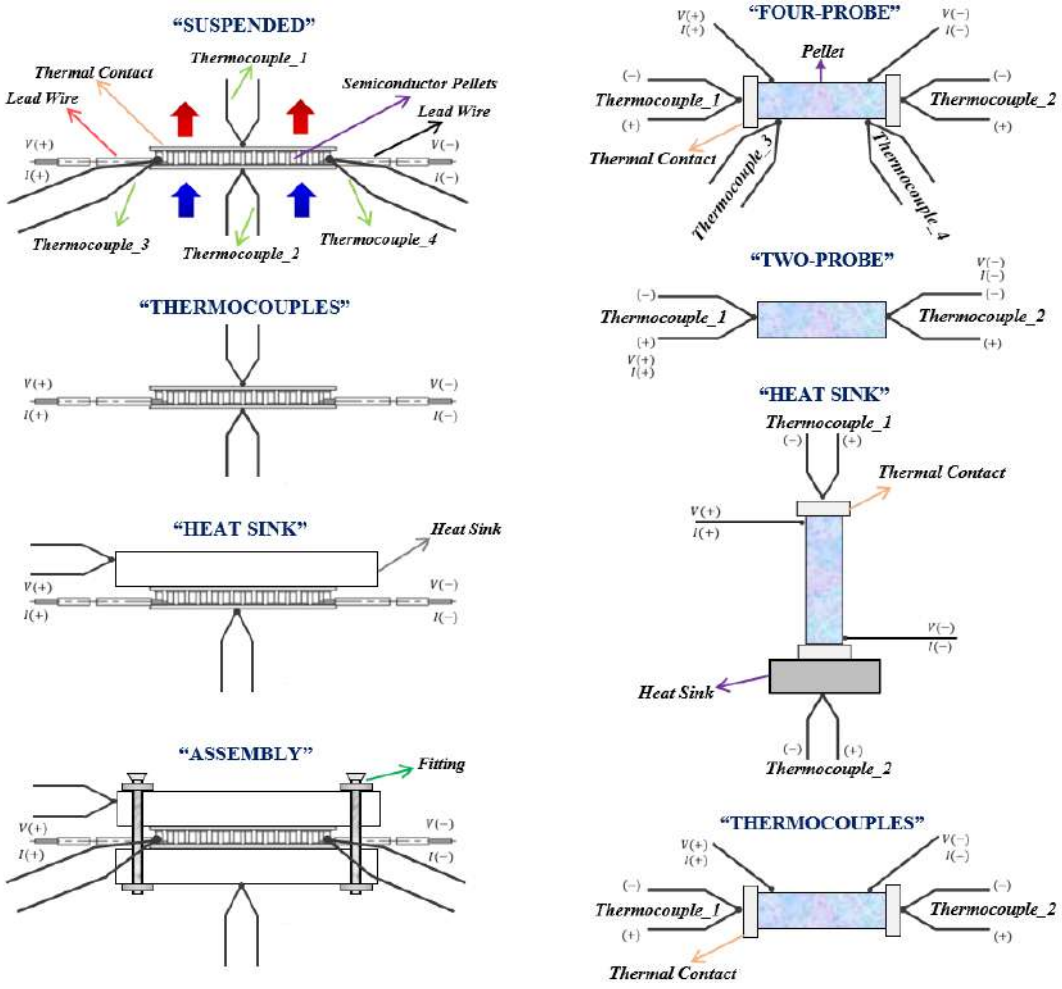

(a) (b)

Fig 1. Characterization configurations for thermoelectric modules (a). Characterization configurations for thermoelectric pellets (b).

This test is very effective for screening samples before more rigorous testing. Additionally, with this configuration, the characteristic thermoelectric times and relaxation times can be determined, using τ_{TE}, τ_{th}, and τ_C. Furthermore, since a ± 1.1°C error in the absolute temperature, $\bar{T}$, produces an error of less than 1%, thus reducing the uncertainty of the measurement and the figure of merit, and $Z\bar{T}$ is measurable directly with precision and versatility. The advantage of this configuration for the thermoelectric module testing is that the thermocouples will not be in contact with the active circuit and voltage pick-up will not be a factor.

B. *T*est Configuration for a Thermoelectric Pellet Sample

Fig. 1 (b), illustrates four different test configurations for a thermoelectric pellet sample. The first configuration is a suspended sample using the "*Four Probes*" technique. This test method is necessary whenever the contact resistance is unknown or significant compared to the resistance of the thermoelectric pellet. The difficulties with this configuration are that: (a) current flow through the pellet can be disturbed by the presence of the thermocouples; (b) voltage pick-up in the probes can result in significant errors in the thermocouple readings; (c) precise measurements of the probe separation are usually very difficult to obtain; and (d) the voltage and temperature planes are affected by the probes and, therefore, are not nearly as well defined at the probes as they are at the opposite ends where high-conductivity end caps are applied.

The "*Two Probes*" setup is suggested for most thermoelectric materials where good contacts are relatively easy to achieve. However, care must be taken to place the current and thermocouples on opposite edges of the end caps to avoid voltage pick-up across the thermocouples. Essentially, the thermocouple should not be placed in a position on the end cap where the current lines intersect. The "*Heat Sink*" configuration is practically the same as the "*Four-Probe*" one concerning instrumentation and connections. The "*Thermocouples* " is recommended to measure $Z\bar{T}$, τ_{th}, and the relaxation time of the material; e.g., $5\tau_{th}$.

IV. EXPERIMENTAL RESULTS

To illustrate the characterization and testing of TEMs a commercially available thermoelectric module is considered as a sample, specifically, the Kryotherm TB-127-1.4-1.2, used by Lineykin and Ben-Yaakov [3] [4]; as well as used by Y. Apertet and H. Ouerdane [11]. The parameters at $\Delta T = 70\ K$ are presented in Table 1. And the Kryotherm TB-127-1.0-1.2 module was also tested [25].

Table1. Parameters at $\Delta T = 70\ K$, $\bar{T} = 300K$, $V_{max} = 15.9\ V$, $I_{max} = 7.6\ A$, $R_{ac}\ (295K) = 1.5\ \Omega$ (Tolerance: +/- 10 %), $Q_{max} = 75\ W$.

$R_m(\Omega)$	$K_0\ (W.K^{-1})$	$C_{th}(J.K^{-1})$	$\alpha\ (V.K^{-1})$	ZT
1.602	0.667	0.35	0.0532	0.795

The Fig. 2 (a), (b), (c), and (d) show the test data taken on TB-127-1.0-1.2 and TB-127-1.4-1.2 using the "*Suspended*" and "*Thermocouples*" configuration without being thermally insulated; that is, in non-adiabatic conditions. The environment was at room temperature $\bar{T} = 300K$, to which the module thermal contacts were exposed. For the temperature measurements, two special type K thermocouples were used, with an error (*Special Limits Error*) of either +/- 0.25 ℃ or $+/-$ 0.4 %. The measurement process used is similar to the one proposed by Buist in [20]. The results obtained for TB-127-1.4-1.2 at $\Delta T = 70\ K$ are shown in the Table 2, and can be compared with Table I. Additionally, analyzing the data taken on both TEM has been possible to distinguish that using the same power supply values setup (voltage, current, and time step) [25], either the TB-127-1.0-1.2 and the TB-127-1.4-1.2 showed different thermoelectric parameters. The errors are associated with the offset of thermocouples and the time step of the power source.

Table 2. Parameters at $\Delta T = 69.25\ K$, $\bar{T} = 300K$, $V_{max} = 15.9\ V$, $I_{max} = 7.6\ A$, $R_{ac}\ (295K) = 1.5\ \Omega$ (Tolerance: +/- 10 %), $Q_{max} = 75\ W$.

$R_{TE}(K/W)$	$C_{TE}(J/K)$	$R_m(\Omega)$	$C_{th}(J/K)$	$K_0\ (W/K)$	$\alpha\ (V/K)$	ZT
0.394	2.871	1.592	0.336	0.633	0.0508	0.768

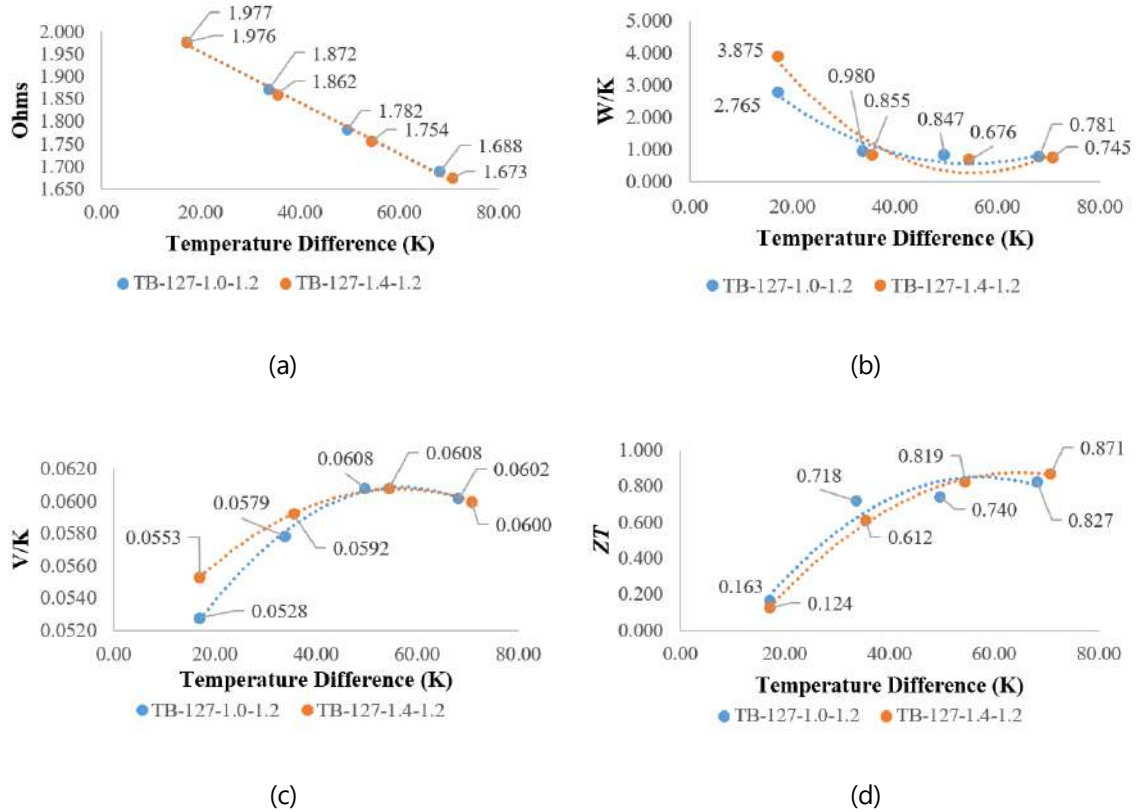

Fig. 2. Electric resistance characterization data taken on TB-127-1.0-1.2 and TB-127-1.4-1.2 (a). Thermoelectric conductance characterization data taken on TB-127-1.0-1.2 and TB-127-1.4-1.2 (b). Seebeck coefficient characterization data taken on TB-127-1.0-1.2 and TB-127-1.4-1.2 (c). Figure of merit characterization data taken on TB-127-1.0-1.2 and TB-127-1.4-1.2 (d).

CONCLUSIONS

The unification of the forced response and natural response theories allows us to describe the complete response of TEMs. From the complete response of TEMs, it has been possible to create the basis to develop and describe in detail a novel methodology for the characterization and testing of thermoelectric materials, pellets, wafers, ingots, modules, and systems. The present method is proven to be fast, accurate, highly appropriate to apply, and conveniently more cost-effective. Using an integrated measurement system that is capable of solving simultaneous the voltage and temperature components of TEMs with high speed and high resolution. Moreover, this methodology provides all the advantageous features of Harman's and Transient's methods. Numerous expressions for the figure of merit expressed as a function of the temperatures were found similar to Harman's and Buist's equations. The methodology provided a direct measurement of the figure of merit with exactness and reproducibility. The subsequent computations yield values for the Seebeck coefficient, electrical resistance, thermal conductance, as well as the famous thermoelectric transport coefficients ρ and κ.

REFERENCES

[1] T. J. Seebeck, «Magnetic polarization of metals and minerals,» *Abhandlungender Deutschen Akademie der Wissenschaften zu Berlin,* vol. 265, 1822-1823.

[2] J. C. Peltier, «Nouvelles experiences sur la caloricite des courans electrique,» *Annales de Chimie et de Physique,* vol. LVI, p. 371–386, 1834.

[3] S. Lineykin e S. Ben-Yaakov, «Analysis of thermoelectric coolers by a spice-compatible equivalent-circuit model,» *IEEE Power Electronics Letters,* vol. 3, n. 2, pp. 63-66, 2005.

[4] S. Lineykin e S. Ben-Yaakov, «Modeling and analysis of thermoelectric modules,» *IEEE Transactions on Industry Applications,* vol. 43, n. 2, pp. 505-512, 2007.

[5] D. M. Rowe, CRC Handbook of Thermoelectrics, Boca Raton: Taylor & Francis, 1995, pp. 192-212.

[6] Z. Ren, Y. Lan e Q. Zhang, Advanced Thermoelectrics Materials, Contacts, Devices, and Systems, Boca Raton: Taylor & Francis Group, LLC, 2018.

[7] N. M. Ravindra, B. Jariwala, A. Bañobre e A. Maske, Thermoelectrics Fundamentals, Materials Selection, Properties, and Performance, Cham: Springer Nature, 2019.

[8] S. LeBlanc, S. K. Yee, M. L. Scullin, C. Dames e K. E. Goodson, «Material and manufacturing cost considerations for thermoelectrics,» *Renewable and Sustainable Energy Reviews,* vol. 32, pp. 313-327, 2014.

[9] S. K. Yee, S. LeBlanc, K. E. Goodson e C. Dames, «$ per W metrics for thermoelectric power generation: beyond ZT,» *Energy & Environmental Science,* vol. 6, n. 9, pp. 2561-2571, 2013.

[10] H. Wang, S. Bai, L. Chen, A. Cuenat, G. Joshi, H. Kleinke, J. König, H. W. Lee, J. Martin, M. W. Oh e W. D. Poter, «International round-robin study of the thermoelectric transport properties of an n-Type half-heusler compound from 300 K to 773 K,» *Journal of Electronic Materials,* vol. 44, n. 11, pp. 4482-4491, 2015.

[11] Y. Apertet e H. Ouerdane, «Small-signal model for frequency analysis of thermoelectric systems,» *Energy Conversion and Management,* vol. 149, pp. 564-569, 2017.

[12] A. F. Ioffe, Physics of Semiconductors, London: Infosearch, 1960.

[13] T. M. Tritt, «Measurement and Characterization Techniques for Thermoelectric Materials,» *MRS Online Proceedings Library (OPL),* vol. 478, 1997.

[14] Z. Zhou e C. Uher, «Apparatus for Seebeck coefficient and electrical resistivity measurements of bulk thermoelectric materials at high temperature,» *Review of scientific instruments,* vol. 76, n. 2, p. 023901, 2005.

[15] T. C. Harman, «Special Techniques for Measurement of Thermoelectric Properties,» *Journal of Applied Physics,* vol. 29, n. 9, pp. 1373-1374, 1958.

[16] T. C. Harman, J. H. Cahn e M. J. Logan, «Measurement of thermal conductivity by utilization of the Peltier effect,» *Journal of Applied Physics,* vol. 30, n. 9, pp. 1351-1359, 1959.

[17] H. Iwasaki, M. Koyano e H. Hori, «Evaluation of the figure of merit on thermoelectric materials by Harman method,» *Japanese Journal of Applied Physics,* vol. 41, n. 11R, p. 6606, 2002.

[18] H. Iwasaki e H. Hori, 24th International Conference on Thermoelectrics, 2005. - Thermoelectric property measurements by the improved Harman method, Clemson, USA: IEEE ICT 2005, 2005, p. 513–516.

[19] R. J. Buist, «A new method for testing thermoelectric materials and devices,» in *11th International Conference on Thermoelectrics*, Arlington, Texas, 1992.

[20] V. Zlatic e R. Monnie, Modern Theory of Thermoelectricity, New York: Oxford University Press, 2014.

[21] J. M. Luttinger, «Theory of thermal transport coefficients,» *Physical Review,* vol. 135, n. 6A, p. A1505, 1964.

[22] R. E. Pirela e S. R. Velásquez, «Forced Response of Thermoelectric Materials and Devices,» *IEEE Latin America Transactions,* vol. 20, n. 8, 2022.

[23] R. E. Pirela e S. R. Velásquez, «Natural Response of Thermoelectric Materials and Devices,» *Athenea Engineering Sciences journal,* vol. 3, n. 10, pp. 49-62, 2022.

[24] Kryotherm Co, «"Thermoelectric coolers for industrial applications: TB-127-1.4-1.2.,» in *Available in: http://www.kryothermtec.com*, Saint-Petersburg, Russia, 2023.

Ronald Edgar Pirela La Cruz was born in Maracaibo, Venezuela in 1983. He received a B.S. degree in Electronic Engineering, a Specialist degree in Digital Telecommunications, and an M.S. degree in Electronic Engineering from the UNEXPO in 2007, 2013 and 2020, respectively. Also, he is currently pursuing a Ph.D. degree in Engineering Sciences at UNEXPO. Currently, he is the Train Lab Engineer in charge of the Train Lab for trains powered by hydrogen, Coradia Stream Project in Alstom Ferroviaria S.P.A., Savigliano, Italia.

Sergio Rafael Velásquez Guzmán - Coautor, received the B.S. degree in Electronic Engineering, from the UNEXPO, in 2008. M.S. degree in Education from UPEL in 2011, an M.S. degree in Electronic Engineering from UNEXPO, in 2012, an MBA degree from UNY in 2014, a Doctor of Education degree in 2015 from UPEL, and a Doctor of Engineering Sciences from UNEXPO in 2019. He is a type B Research Professor accredited by the MINCYT in Venezuela. Currently, he is in charge of the Research and Postgraduate Department of the UNEXPO Vice-Rectorate, Puerto Ordaz, Venezuela.

$$(x+a)^n = \sum_{k=0}^{n} \binom{n}{k} x^k a^{n-k}$$

$$(1+x)^n = 1 + \frac{nx}{1!} + \frac{n(n-1)x^2}{2!} + \cdots$$

Published by:

AutanaBooks
Engineering & Services